ARTICLES

Journal of Semiconductors
(2019) 40, 092001
doi: 10.1088/1674-4926/40/9/092001

Broadband polarized photodetector based on p-BP/n-ReS_2 heterojunction

Wenkai Zhu[1, 2], Xia Wei[1, 2], Faguang Yan[1, 2], Quanshan Lv[1, 2], Ce Hu[1, 2], and Kaiyou Wang[1, 2, 3, 4, †]

[1]State Key Laboratory of Superlattices and Microstructures, Institute of Semiconductors, Chinese Academy of Sciences, Beijing 100083, China
[2]Center of Materials Science and Optoelectronics Engineering, University of Chinese Academy of Sciences, Beijing 100049, China
[3]Center for Excellence in Topological Quantum Computation, University of Chinese Academy of Science, Beijing 100049, China
[4]Beijing Academy of Quantum Information Sciences, Beijing 100193, China

Abstract: Two-dimensional (2D) atomic crystals, such as graphene, black phosphorus (BP) and transition metal dichalcogenides (TMDCs) are attractive for use in optoelectronic devices, due to their unique crystal structures and optical absorption properties. In this study, we fabricated BP/ReS_2 van der Waals (vdWs) heterojunction devices. The devices realized broadband photoresponse from visible to near infrared (NIR) (400–1800 nm) with stable and repeatable photoswitch characteristics, and the photoresponsivity reached 1.8 mA/W at 1550 nm. In addition, the polarization sensitive detection in the visible to NIR spectrum (532–1750 nm) was demonstrated, and the photodetector showed a highly polarization sensitive photocurrent with an anisotropy ratio as high as 6.44 at 1064 nm. Our study shows that van der Waals heterojunction is an effective way to realize the broadband polarization sensitive photodetection, which is of great significance to the realization and application of multi-functional devices based on 2D vdWs heterostructures.

Key words: broadband; polarized photodetection; p-BP/n-ReS_2; vdWs herterojunction broadband; polarized photodetection; vdWs heterojunction

Citation: W K Zhu, X Wei, F G Yan, Q Lv, C Hu, and K Y Wang, Broadband polarized photodetector based on p-BP/n-ReS_2 heterojunction[J]. *J. Semicond.*, 2019, 40(9), 092001. http://doi.org/10.1088/1674-4926/40/9/092001

1. Introduction

Two dimensional (2D) van der Waals (vdWs) crystals, such as graphene[1], black phosphorus (BP)[2], silicene[3], group-IV monochalcogenides[4] and transition metal dichalcogenides (TMDCs)[5], are attractive for use in various field, such as electronics and optoelectronics[6–8], valleytronics[9], flexible devices[10], memory devices[11], sensors[12], due to their unique electronic, mechanical, thermal, optical properties. The vdWs crystals have atomically flat thickness and clean interfaces that are free of dangling bonds due to relatively weak van der Waals interactions among layers. This offers opportunities to stack different individual 2D materials into vdWs heterostructures without the limitations of lattice mismatch. The vdWs heterostructures have opened a new platform for fundamental research and device applications[13]. Broadband photodetector have great potential for optoelectronic applications, such as optical communication, imaging, night vision, environmental monitoring, and remote sensing[14–18]. Polarization properties is another degree of freedom for light that is largely uncorrelated with spectral and intensity images, and thus has the ability to carry more information[16]. Therefore, the broadband polarization sensitive photodetector based on vdWs structure will promote the development of the next generation photodetectors.

Black phosphorus is a layered material, where each phosphorus atom is bonded covalently to three neighboring atoms forming a puckered orthorhombic lattice. The BP is a direct bandgap semiconductor. The band gap of BP is dependent on the number of layers, which increases from ~0.3 eV for bulk to ~2 eV for monolayer limit[19]. The ultrahigh carrier mobility of ~1000 $cm^2V^{-1}s^{-1}$ was obtained in BP field effect transistor (FET) for a thickness of ~10 nm[2]. BP also has high in-plane anisotropy properties due to its different bond angles and lengths along the direction of armchair (AC) and zigzag (Z Z)[20, 21]. The hole mobility of BP can theoretically reach 10 000 to 26 000 $cm^2V^{-1}s^{-1}$ for the monolayer (ZZ direction)[22]. Polarization sensitive broadband photodetectors based on BP FET have been demonstrated, which indicating BP is a promising candidate for broadband polarization sensitive photodetection[23].

Rhenium disulphide (ReS_2) as a member of TMDCs also have been extensively investigated[24, 25]. ReS_2 is a semiconductor with a single direct band gap of 1.55 eV that is nearly independent of the number of atomic layers[26, 27]. It exhibits a strong in-plane anisotropy in nature due to its stable Peierls distorted octahedral (1*T*) phase where the buckled S layers and zigzag Re chains along one of the lattice vectors in the plane[26, 28]. According to the reported ReS_2 photodetectors, it shows an n-type behavior with the electron mobility of ~40 $cm^2V^{-1}s^{-1}$, and a photoresponsivity of 10^3 A/W was achieved at low intensity of light, which implies ReS_2 has a potential for sensitive photodetection[29, 30].

Recently, the reported BP-on-WSe_2 heterostructure photodetector exhibits a broadband photoresponsivity in a spectral range of 400–1550 nm[19]. A similar photodetectors based on

Correspondence to: K Y Wang, kywang@semi.ac.cn
Received 29 JUNE 2019; Revised 5 JULY 2019.

BP/ReS_2 p–n diode were reported, which shows the photoresponse properties can be modified by adjusting the back gate voltage, however a high photoresponsivity achieved only in the ultraviolet (UV) band[31]. Another photodetector based on BP/ReS_2 heterojunctions were stacked by controlling their crystal orientation, which exhibits a stronger polarization-dependent photocurrent characteristic in the visible region[32]. In this work, we systematically studied the variation of photoresponsivity and the polarization sensitive photocurrent anisotropy ratio of the BP/ReS_2 heterojunction devices with the incident light power and wavelength. The devices realize broadband photoresponse from visible to near infrared (NIR) (400–1800 nm) with stable and repeatable photoswitch characteristics, and the photoresponsivities reaches 1.8 mA/W at 1550 nm. In addition, the polarization sensitive detection from the visible to NIR spectrum (532–1750 nm) was demonstrated, which shows a highly polarization sensitive photocurrent with an anisotropy ratio as high as 2.98 at 532 nm, 3.39 at 650 nm, 6.44 at 1064 nm, 5.5 at 1550 nm, and 4.3 at 1750 nm. Our study shows that the vdWs heterojunctions is an effective way to realize the broadband and polarized photodetection.

2. Experiments

Fabrication of the BP/ReS_2 heterojunction-based polarized photodetector devices. First, a BP (from HQ graphene) flake was exfoliated onto polydimethylsiloxane (PDMS) stamps by adhesive tape. The stamps are adhered to a glass slide. Under optical microscope, the BP flake with appropriate thickness and shape can be chosen. Afterwards, the target BP flake was transferred onto a 300 nm thick SiO_2/Si substrate by using a site-controllable dry transfer method[33]. Then, using the same method, a ReS_2 (from HQ graphene) flake was transferred onto the BP flake to fabricate a 2D heterojunction. Notably, the whole transfer processes were performed in a glove box to ensure a clean interface. Finally, the source and drain electrode regions were patterned by standard electron beam lithography, and Ta/Au (5/45 nm) layers were deposited on an ultrahigh vacuum evaporative sputtering system, followed by a lift-off process. The lift-off process was also performed in a glove box to avoid BP degradation. The thickness of both BP and ReS_2 flakes were measured by atomic force microscopy (AFM) (Bruker Multimode 8). The device was stored in a small vacuum chamber with 2×10^{-5} mbar during the whole electric and optoelectric measurement processes.

Electrical and optoelectrical properties were measured using a semiconductor characterization system (Agilent Technology B1500A) and a lock-in amplifier (SR830) with a light chopper. The visible to NIR light illumination was provided by a Fianium WhiteLase supercontinuum laser source. The output light was tuned into monochromatic light by an Omni-λ300 monochromator. For the spatially-dependent photocurrent measurement, a microscope objective lens (50×), a lock-in amplifier (SR830) with a light chopper and a micromechanical stage were combined. Linearly polarized light was obtained by making a laser beam pass through a Glan-Taylor prism (polarizer) and a half-wave plate (HWP). The polarization direction of the light was controlled by rotating the HWP while keeping the incident laser power a constant.

Calculation details of the FET device mobility: The field-effect mobility can be calculated using the equation $\mu = (L/W)(d/\varepsilon_0\varepsilon_r V_{ds})(\Delta I_{ds}/\Delta V_{bg})$, where L and W are the length and width of the channel respectively, d is the oxide thickness, ε_0 and ε_r are the permittivity of free space and the relative permittivity of the SiO_2, and the last term is the slope of the transfer curve in the linear regime of the ON state.

3. Results and discussion

Characteristic of the BP/ReS_2 heterojunction device. Fig. 1(a) presents a schematic of our heterojunction device. All of the devices were prepared by mechanical exfoliation and site-controllable dry transfer method. The detailed fabrication processes has been provided in the experimental section. An AFM image of the p-BP/n-ReS_2 heterojunction is shown in Fig. 1(b), with the height profile along the red solid line being shown in the inset, indicating the thicknesses of BP (~10 nm) and ReS_2 (~12 nm). We first performed the electrical characterizations of the ReS_2 FET and BP FET at room temperature. Fig. 1(c) shows the transfer curve of the ReS_2 FET with a linear plot of the source-drain current (I_{ds}) versus back gate voltage (V_{bg}) at a fixed source–drain voltage (V_{ds} = 0.5 V). The device shows an n-type FET behaviors with electron mobility of ~29 $cm^2V^{-1}s^{-1}$ (see the experimental section for the calculation details), which is consistent with the reported value[30]. Optical microscope image of the ReS_2 FET covered by ~10 nm thick BN is shown in the top inset of Fig. 1(c). The thickness of the ReS_2 is about 6 nm. The I_{ds}–V_{ds} curves under different V_{bg} for the ReS_2 FET have been presented in the bottom inset of Fig. 1(c). The linear I_{ds}–V_{ds} curves under low drain voltage indicates negligible Schottky barrier at the ReS_2 and Au interfaces. Fig. 1(d) shows I_{ds} as a function of V_{bg} for BP FET at room temperature and V_{ds} = 0.5 V. This device showed a p-type FET behavior with hole mobility ~ 166 $cm^2V^{-1}s^{-1}$. The top inset of Fig. 1(d) shows the optical microscope image of the BP FET covered by ~15 nm thick BN. The thickness of the BP is about 10 nm. The I_{ds}–V_{ds} curve of the BP FET is shown in the bottom inset of Fig. 1(d). The near-linear I_{ds}–V_{ds} curve shows a near ohmic contact between BP and Au.

In addition to the conductive type of the materials, the energy band structure of the materials is also very important for construction of a p–n junction. The energy band diagrams of the heterojunction in the isolated and different bias states are illustrated in Figs. 2(a)–2(d). Based on previous reports, the electron affinity and bandgap (E_g) of multilayer BP are around 4.2 and 0.4 eV, respectively[20, 22, 34]. For multilayer ReS_2, the corresponding values are about 4.4 and 1.55 eV[26, 32]. Therefore, the BP/ReS_2 heterojunction has a type-II band alignment because the conduction band minimum (E_C) of BP lies above that of ReS_2 by ΔE_C = 0.2 eV, whereas the valence band maximum (E_V) of ReS_2 lies below (ΔE_V = 1.35 eV) that of BP. In addition, the valence band edge of BP lies below that of the conduction band edge of ReS_2 by only 0.2 eV, which means the BP/ReS_2 heterojunction can be easily electrostatic tuned to a broken-gap heterojunction with type-III band alignment, which can be used to explore the TFETs[35, 36]. Fig. 2(a) presents the band diagram for isolated few layers p-BP and n-ReS_2. The built-in potential is formed when the two-layered materials are stacked together, which is indicated by blue arrow in Fig. 2(b). At V_{ds} = 0 V, the minority carrier (electron) in BP crosses the small barrier and forms a small reverse current. As shown in Fig. 2(c), under positive bias, the electrons (majority carriers in ReS_2) will trans-

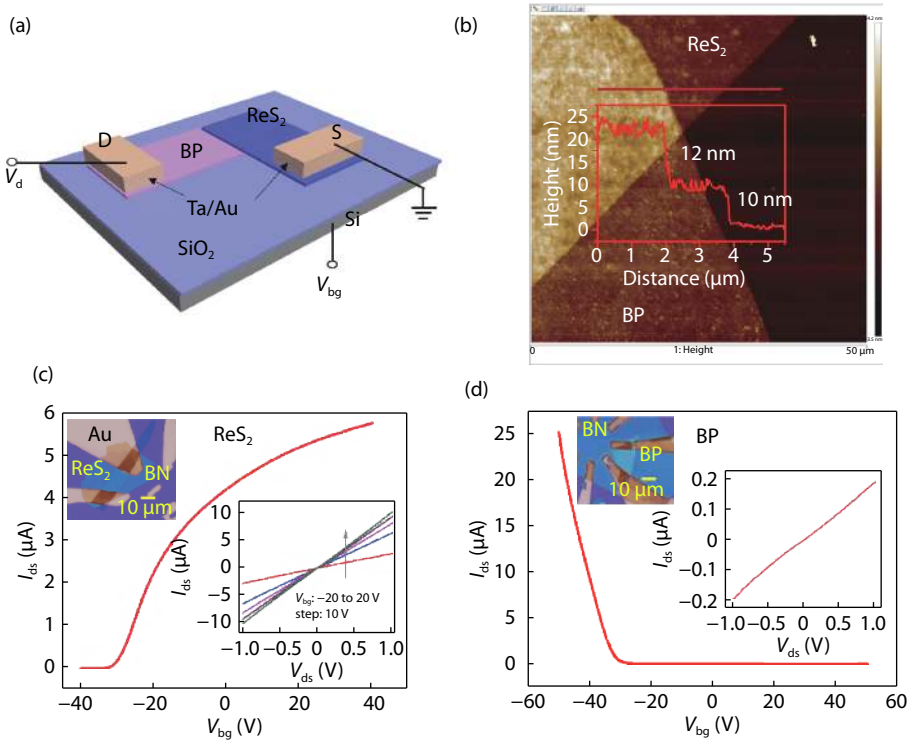

Fig. 1. (Color online) (a) Structure schematic of BP/ReS_2 heterojunction device. The source electrode (the contact connected to ReS_2) is grounded. The drain electrode (the contact connected to BP) is applied a voltage V_d. (b) AFM image of p-BP/n-ReS_2 heterojunction device. The inset shows the height profile along the red solid line, indicating the thicknesses of BP (~10 nm) and ReS_2 (~12 nm). (c) The transfer curve of the ReS_2 FET with Au contact was measured at room temperature and V_{ds} = 0.5 V. Top inset: Optical microscope image of the ReS_2 FET. The scale bar is 10 μm. The thickness of the ReS_2 is about 6 nm. Bottom inset: Current–voltage (I_{ds}–V_{ds}) curves for different gate voltages (V_{bg}). (d) I_{ds} as a function of V_{bg} for BP FET at room temperature and V_{ds} = 0.5 V. Top inset: Optical microscope image of the BP FET. The thickness of the BP is about 10 nm. Bottom inset: I_{ds}–V_{ds} curve of the BP FET.

port to BP by overcoming the barrier height ΔE_1. Meanwhile, the holes (majority carriers in BP) will travel to ReS_2 by overcoming the barrier height ΔE_2. Due to the larger ΔE_2 compare to ΔE_1, the current is dominated by the over-barrier free-electron transport (blue arrow). Fig. 2(d) shows the electrical field in the heterojunction is strongly enhanced under reverse bias. The minority carrier (electrons in BP and holes in ReS_2) contributes to the conduction process.

To investigate the responsivity of the device dependence on the illumination intensities, different illumination intensities P ranging from 0 to 500 W/cm^2 are applied to the heterojunction device. Fig. 3(a) shows the $|I_{ds}|$–V_{ds} curves of the BP/ReS_2 heterojunction device at room temperature in the dark and under illumination with a 1550 nm laser at various excitation intensities (P = 10, 25, 50, 100, 250, 500 W/cm^2). The $|I_{ds}|$–V_{ds} curve of the device in the dark exhibits a clear rectifying behavior. The rectification ratio, defined as the ratio of the forward/reverse current, is about 50 at V_{ds} = +1/–1 V. This behavior can be attributed to the formation of p–n diode within the atomically thin BP/ReS_2 heterojunction (more details see band alignment of the BP/ReS_2 heterojunction). The device exhibits a low dark current (~1.0 nA) at V_{ds} = –1 V. Under a light illumination, electron-hole pairs are generated and separated by the electric field in the heterojunction, which generate the photocurrents. Photocurrent (I_{ph}) is defined as the difference between drain currents with and without light-illumination ($I_{ph} = |I_{light} - I_{dark}|$). Under reverse bias ($V_{ds}$ < 0 V), I_{ph} increases with increasing the light intensity P. I_{ph} can also be enhanced by increasing the reverse bias (shown in Fig. 3(b)). It can be explained by the increased electrical field in the heterojunction under reverse bias (Fig. 2(d)). The increased electrical field decreases the carrier transit time, thus reduces the recombination probability of the photo-generated electrons and holes. In addition, I_{ph} exhibits a sublinear dependence on the incident light intensity P and follows a power law of $I_{ph} \propto P^{\alpha}$, where α = 0.61, 0.68, and 0.73 at V_{ds} = 0, –0.4 and –1 V, respectively. Larger value α can be obtained by applied a larger reverse bias, which also benefits from the shorter carrier transit time. The similar sublinear behavior has also been reported for other similar structures, such as ReS_2 FETs[29], WSe_2/graphene[37], MoS_2/WS_2 heterostrctures[38], and several of our previous works (WS_2/GaSe, InSe/GaSe, WSe_2/GaSe, $MoTe_2$ photodetectors)[39–42]. To quantify the photoresponse performance, the photoresponsivity ($R = I_{ph}/PS$) of the heterojunction as a function of the illumination intensity at different applied voltages were extracted and shown in Fig. 3(c). The corresponding external quantum efficiency (EQE = $hcR/e\lambda$) of the device at different V_{ds} (V_{ds} = 0, –0.4, –1 V) were presented in Fig. 3(d). Here S is the in-plane area (~20 μm^2) of the device, e is the electron charge, c is the speed of the light and h is Planck constant. All of two important factors increase with decreasing light intensity, consistent with the sublinear behavior of the photocurrent. Our device exhibits a photoresponsivity of R = 1.8 mA/W with corresponding EQE = 0.14% at V_{ds} = –1 V under the wavelength 1550 nm. The photoresponsivity is comparable to most of similar vdWs heterojunction photodetectors reported recently, such as 4.36 mA/W

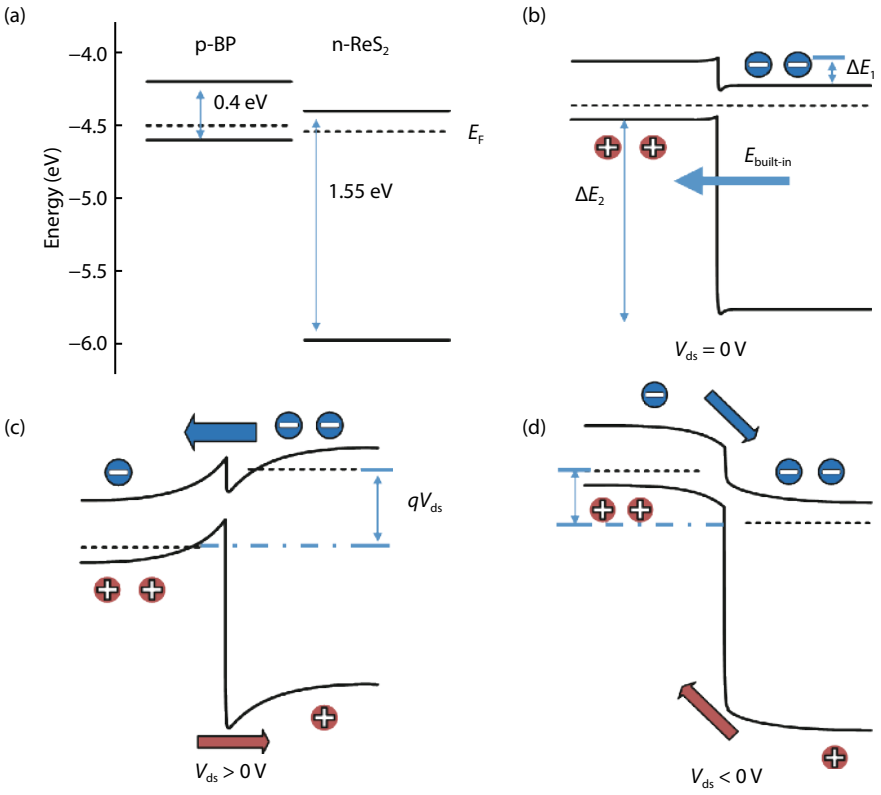

Fig. 2. (Color online) (a) Band alignment for isolated p-BP and n-ReS_2 layers. Electron affinities of BP and ReS_2 are around 4.2 and 4.4 eV, respectively. (b–d) schematic band diagrams at the interface of the BP/ReS_2 heterojunction at different applied voltages V_{ds} ((b)zero bias, (c) positive bias and (d) negative bias). The transportation of electrons and holes are indicated by blue arrows and red arrows, respectively.

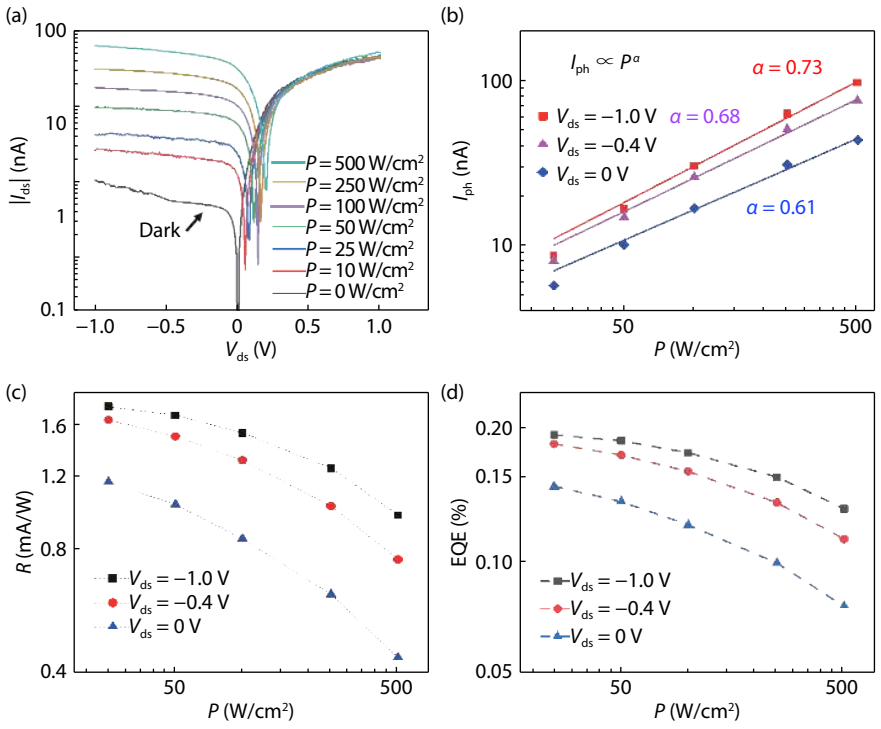

Fig. 3. (Color online) (a) $|I_{ds}|$–V_{ds} curves of the BP/ReS_2 heterojunction device at room temperature in the dark and under illumination with a 1550 nm laser at various excitation intensities (P = 10, 25, 50, 100, 250, 500 W/cm^2). (b) Photocurrent as a function of the illumination intensity at different V_{ds} (V_{ds} = 0, –0.4, –1 V). The solid lines are fits to the data. (c) Photoresponsivity (R) of the BP/ReS_2 heterojunction device as a function of the illumination intensity at different V_{ds} (V_{ds} = 0, –0.4, –1 V). (d) The external quantum efficiency, EQE, of the heterojunction device as a function of the illumination intensity P at different V_{ds} (V_{ds} = 0, –0.4, –1 V). The wavelength of incident light is 1550 nm.

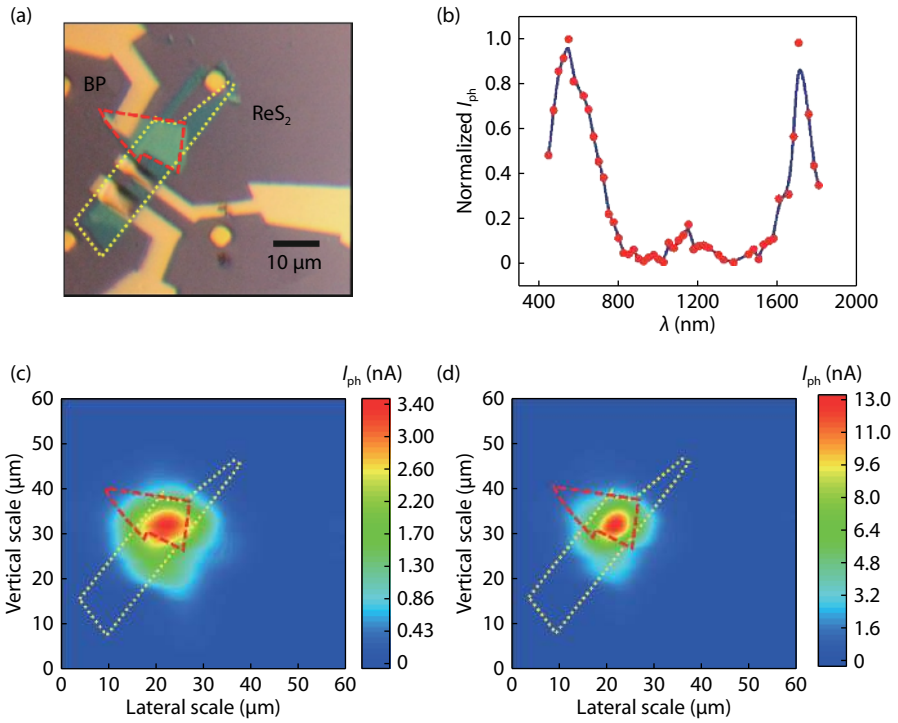

Fig. 4. (Color online) (a) Optical microscope image of the BP/ReS_2 heterojunction device, component materials are outlined in different colors. (b) The normalized photocurrent as a function of the illumination wavelength at V_{ds} = –1 V and illumination intensity P = 100 W/cm^2. (c), (d) Scanning photocurrent microscope images of the BP/ReS_2 heterojunction at V_{ds} = 0 V (c) and –1 V (d) with illumination wavelength 1550 nm (illumination intensity P = 100 W/ cm^2). The red dotted line outlines the BP flake and yellow dotted line outlines the ReS_2 flake, respectively. The laser beam is focused by microscope objective lens (50×) and the diameter of the spot size is about 5 μm.

in MoS_2/WS_2[43].

The image of the BP/ReS_2 heterojunction device shown in Fig. 4(a), where the boundaries of each layer are indicated by dotted lines with different colors. The corresponding scale bar is 10 μm. Fig. 4(b) shows the normalized photocurrent as a function of the illumination wavelength at V_{ds} = –1 V and illumination intensity P = 100 W/cm^2, which demonstrates the BP/ReS_2 heterojunction device exhibits obvious photoresponse over a broad spectral range (400–1800 nm), from the visible to near infrared. The maximum normalized I_{ph} ~ 1 is obtained at wavelength of 550 nm, and the minimum normalized I_{ph} ~ 0.013 is obtained at wavelength of 1025 nm. Therefore, the device can be used for broadband photodetection. ReS_2 has the strongest absorption in the ultraviolet and visible band, but weaker absorption in the near infrared bands[44]. Meanwhile, BP has a natural narrow band gap, which has a strong absorption in visible and near infrared bands. As a result, a strong absorption at 550 nm of the device is induced by the light absorption properties of ReS_2 and BP. Another strong absorption at 1710 nm of the device is dominated by the light absorption properties of BP. According to the reported results, the absorption peak position for a N-layer BP can be described using tight-binding model through the expression $E_{N,n} = 1.8 - 1.46\cos(n\pi/(N+1))$, where the subband index n = 1…N[45]. The absorption peaks of 550 nm (2.25 eV) and 1720 nm (0.72 eV) in our device can be explained by n = 13, 5 when L = 20. In order to explore the origin of the photoresponse, scanning photocurrent maps were measured at both zero and negative biases. The corresponding photocurrent maps at zero and negative biases with 1550 nm laser excitation (illumination intensity P = 100 W/cm^2) are shown in Figs. 4(c) and 4(d), respectively. The photocurrent map shows that the photoresponse of the overlapping region is strongly enhanced compared with the non-overlapping regions. It also demonstrates the formation of a p–n junction across the area of the BP/ReS_2 interface where the photo-generated electrons and holes are separated and extracted more efficiently.

The excellent stability is an important condition for the application of photodetectors. For investigate the stability of the device, the device was illuminated by a laser with different wavelength (or under different V_{ds}) and light intensity P = 50 W/cm^2. Fig. 5(a) presents the time dependences of $|I_{ds}|$ during incident light switched on/off at V_{ds} = –1 V with different wavelength (λ = 400, 532, 1064, 1320, 1550 nm), which shows the device can steady working over a broad spectral range, from visible to near infrared. In addition, the photoswitch ratio (I_{light}/I_{dark}) of the device is about 23 at 400 nm, 25 at 532 nm, 12 at 1064, 13 at 1320, and 7 at 1550 nm. Source–drain current $|I_{ds}|$ as a function of time with photoswitching at different V_{ds} (V_{ds} = 0, –0.2, –0.4, –0.6, –0.8, –1 V) shown in the Fig. 5(b). A stabilized photoresponsivity ~ 0.4 mA/W was achieved at λ = 1550 nm under zero bias, which shows the device can work as a self-driven near infrared photodetectors. Moreover, after many cycles, the photocurrent still responds in a similar fashion to the light, which exhibits excellent operation reversibility and stability.

To examine the polarization sensitivity of the device, the device was illuminated by linearly polarized light with different polarized angle. The photocurrent as a function of polarized angle under different illumination wavelength is shown in Fig. 6. The optical microscope image of the BP/ReS_2 heterojunction device is exhibited in Fig. 6(a). The angles of zero

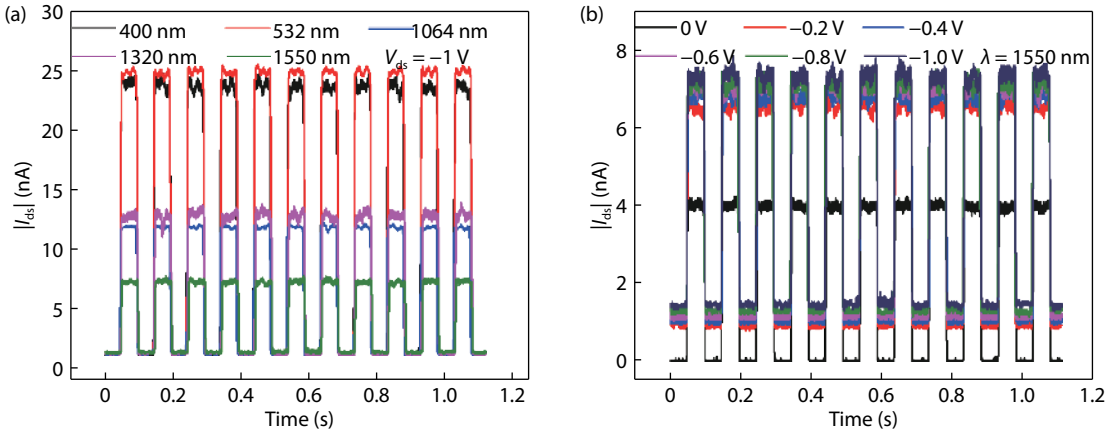

Fig. 5. (Color online) (a) Time dependences of I_{ds} during incident light switched on/off at V_{ds} = –1 V with different wavelength (λ = 400, 532, 1064, 1320, 1550 nm). (b) Source–drain current I_{ds} as a function of time with photoswitching at different V_{ds} (V_{ds} = 0, –0.2, –0.4, –0.6, –0.8, –1 V). The light intensity P = 50 W/cm^2.

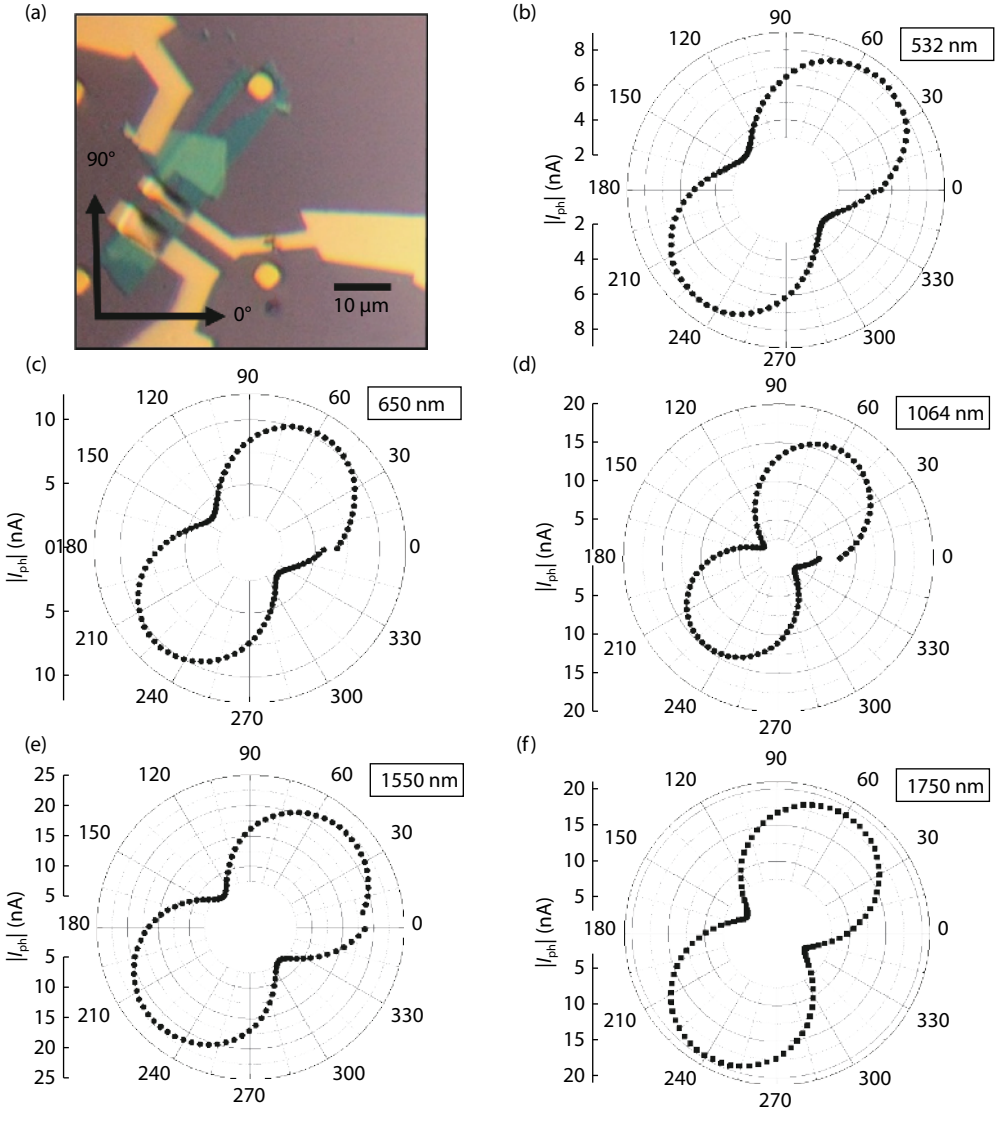

Fig. 6. (Color online) (a) Optical microscope image of the BP/ReS_2 heterojunction device. The angles of zero degree and 90 degree represents the rotation direction of the linearly polarized light. (b), (c) The anisotropic response in I_{ph} plotted in the polar coordination at visible light wavelength of 532 and 650 nm. The visible light intensity P = 25 W cm^2. (d–f) The evolution of the I_{ph} plotted in the polar coordination at near infrared light wavelength of (d) 1064 nm, (e) 1550 nm, and (f) 1750 nm. The near infrared light intensity P = 100 W/ cm^2. The V_{ds} is fixed in –1 V.

degree and 90 degree represents the rotation direction of the linearly polarized light. The anisotropic response in $|I_{ph}|$ plotted in the polar coordination at visible light wavelength of 532 nm (Fig. 6(b)) and 650 nm (Fig. 6(c)). The visible light intensity $P = 25$ W/cm^2. Figs. 6(d)–6(f) presents the evolution of the $|I_{ph}|$ plotted in the polar coordination at near infrared light wavelength of 1064 nm (Fig. 6(d)), 1550 nm (Fig. 6(e)), and 1750 nm (Fig. 6(f)). The near infrared light intensity $P = 100$ W/cm^2. The results show the device can act as a polarized photodetector over a broad spectral range (from 532 to 1750 nm). The double symmetry has been observed. The direction of the maximum photocurrent is perpendicular to the direction of the minimum photocurrent. The polarization sensitive absorption of the BP/ReS_2 heterojunction photodetector is induced by crystal structure anisotropy. Because of the intrinsic low carrier mobility and high electron–hole recombination rate in ReS_2[29], the polarization sensitivity of ReS_2 is relatively low. Thus, the polarization sensitive absorption of the BP/ReS_2 heterojunction device is mainly induced by crystal structure anisotropy of BP. The absorption of armchair-polarized light is always stronger than zigzag-polarized light for BP with all thicknesses, thus the two directions of the maximum photocurrent difference correspond to the orientation of BP crystal[45, 46]. It is worth noting the polarized photocurrent ratio $I_{ph.max}/I_{ph.min} \approx$ 2.98 at 532 nm, 3.39 at 650 nm, 6.44 at 1064 nm, 5.5 at 1550 nm, 4.3 at 1750 nm, which is larger than some other polarized sensitive anisotropy photodetectors, such as GeSe (1.09 at 532 nm)[47] and BP vertical p-n junction (3.5 at 1200 nm)[23]. The electrons transition process must meet the transition selection rule of momentum conservation, which can be expressed by the formulas: $E_g = \hbar\omega$ and $\hbar k_i \pm \hbar q_{phonon} = \hbar k_f$, where E_g is the bandgap of the semiconductor, k_i and k_f are the electron wave vectors at the valence band maximum (VBM) and conduction band minimum (CBM), respectively, ω is the angular frequency of the incident photon. In addition, the electric dipole transition probability $P(\omega)$ for photon absorption per unit time is introduced by Fermi Golden Rule: $P(\omega) = 2\pi/\hbar|\langle\varphi_f|H_{eR}|\varphi_i\rangle|^2\delta(E(k_f) - E(k_i) - \hbar\omega)$, where $\hbar$ is the reduced Plank constant, H_{eR} is the interaction of electromagnetic excitation. Here the transition occur from the initial states $|\varphi_i\rangle$ to the finial states $|\varphi_f\rangle$ with corresponding energy level $E(k_i)$ and $E(k_f)$. Moreover, the distribution and the overlap of VBM and CBM wave function is different along zigzag and armchair direction in BP, which will result in the difference of the $|\langle\varphi_f|H_{eR}|\varphi_i\rangle|^2$ value[47] and wavelength dependent polarized photoresponse. In the near infrared region, BP has a large photoresponse to the polarized light along the armchair direction while the photoresponse of polarized light along the zigzag direction is small and changes little[23]. Thus the large polarized photocurrent ratios are observed in the near infrared region and the maximum polarized photocurrent ratio is 6.44 at 1064 nm.

4. Conclusion

In conclusion, we have fabricated BP/ReS_2 vdWs heterojunction devices by dry-transfer of 2D flakes method. The devices realize broadband photoresponse from visible to near infrared (NIR) (400–1800 nm) with stable and repeatable photoswitch characteristics, and the photoresponsivities reached 1.8 mA/W at 1550 nm. In addition, the polarization sensitive detection form the visible to NIR spectrum (532–1750 nm) was demonstrated, which shows a highly polarization sensitive photocurrent with an anisotropy ratio as high as 2.98 at 532 nm, 3.39 at 650 nm, 6.44 at 1064 nm, 5.5 at 1550 nm, and 4.3 at 1750 nm. Because of the intrinsic low carrier mobility and high electron–hole recombination rate in ReS_2, the polarization sensitivity of ReS_2 is relatively low. Thus, the polarization sensitive absorption of the BP/ReS_2 heterojunction device is mainly induced by crystal structure anisotropy of BP. Our study shows that van der Waals heterojunction is an effective way to realize the broadband polarization sensitive photodetection, which is of great significance to the application of multi-functional devices based on 2D vdWs heterostructures.

Acknowledgements

This work was supported by the National Key R&D Program of China (Grant No. 2017YFA0303400 and No.2017YFB 0405700). This work was also supported by the NSFC Grant Nos. 61774144 and 11474272. The project was sponsored by Chinese Academy of Sciences, grant No. QYZDY-SSW-JSC020, XDPB12, and XDB28000000.

References

[1] Novoselov K S, Geim A K, Morozov S V, et al. Electric field effect in atomically thin carbon films. Science, 2004, 306(5696), 666
[2] Li L, Yu Y, Ye G J, et al. Black phosphorus field-effect transistors. Nat Nanotechnol, 2014, 9, 372
[3] Vogt P, De Padova P, Quaresima C, et al. Silicene: compelling experimental evidence for graphenelike two-dimensional silicon. Phys Rev Lett, 2012, 108(15), 155501
[4] Gomes L C, Carvalho A. Phosphorene analogues: Isoelectronic two-dimensional group-IV monochalcogenides with orthorhombic structure. Phys Rev B, 2015, 92(8), 085406
[5] Splendiani A, Sun L, Zhang Y, et al. Emerging photoluminescence in monolayer MoS_2. Nano Lett, 2010, 10(4), 1271
[6] Wang Q H, Kalantar-Zadeh K, Kis A, et al. Electronics and optoelectronics of two-dimensional transition metal dichalcogenides. Nat Nanotechnol, 2012, 7, 699
[7] Cao Y, Cai K, Hu P, et al. Strong enhancement of photoresponsivity with shrinking the electrodes spacing in few layer GaSe photodetectors. Sci Rep, 2015, 5, 8130
[8] Luo W, Cao Y, Hu P, et al. Gate tuning of high-performance InSe-based photodetectors using graphene electrodes. Adv Opt Mater, 2015, 3(10), 1418
[9] Schaibley J R, Yu H, Clark G, et al. Valleytronics in 2D materials. Nat Rev Mater, 2016, 1, 16055
[10] Akinwande D, Petrone N, Hone J. Two-dimensional flexible nanoelectronics. Nat Commun, 2014, 5, 5678
[11] Feng Q, Yan F, Luo W, et al. Charge trap memory based on few-layer black phosphorus. Nanoscale, 2016, 8(5), 2686
[12] Rao C N R, Gopalakrishnan K, Maitra U. Comparative study of potential applications of graphene, MoS_2, and other two-dimensional materials in energy devices, sensors, and related areas. ACS Appl Mater Interfaces, 2015, 7(15), 7809
[13] Pizzocchero F, Gammelgaard L, Jessen B S, et al. The hot pick-up technique for batch assembly of van der Waals heterostructures. Nat Commun, 2016, 7, 11894
[14] Konstantatos G, Sargent E H. Nanostructured materials for photon detection. Nat Nanotechnol, 2010, 5, 391
[15] Gong C, Zhang Y, Chen W, et al. Electronic and optoelectronic applications based on 2D novel anisotropic transition metal dichalcogenides. Adv Sci, 2017, 4(12), 1700231
[16] Tyo J S, Goldstein D L, Chenault D B, et al. Review of passive ima-

ging polarimetry for remote sensing applications. Appl Opt, 2006, 45(22), 5453

[17] Yan F, Wei Z, Wei X, et al. Toward high-performance photodetectors based on 2D materials: strategy on methods. Small Methods, 2018, 2(5), 1700349

[18] Wei X, Yan F G, Shen C, et al. Photodetectors based on junctions of two-dimensional transition metal dichalcogenides. Chin Phys B, 2017, 26(3), 038504

[19] Ye L, Wang P, Luo W, et al. Highly polarization sensitive infrared photodetector based on black phosphorus-on-WSe_2 photogate vertical heterostructure. Nano Energy, 2017, 37, 53

[20] Tran V, Soklaski R, Liang Y, et al. Layer-controlled band gap and anisotropic excitons in few-layer black phosphorus. Phys Rev B, 2014, 89(23), 235319

[21] Zhou Z, Cui Y, Tan P H, et al. Optical and electrical properties of two-dimensional anisotropic materials. J Semicond, 2019, 40(6), 061001

[22] Qiao J, Kong X, Hu Z X, et al. High-mobility transport anisotropy and linear dichroism in few-layer black phosphorus. Nat Commun, 2014, 5, 4475

[23] Yuan H, Liu X, Afshinmanesh F, et al. Polarization-sensitive broadband photodetector using a black phosphorus vertical p–n junction. Nat Nanotechnol, 2015, 10, 707

[24] Zhang E, Jin Y, Yuan X, et al. ReS_2-based field-effect transistors and photodetectors. Adv Funct Mater, 2015, 25(26), 4076

[25] Rahman M, Davey K, Qiao S Z. Advent of 2D rhenium disulfide (ReS_2): fundamentals to applications. Adv Funct Mater, 2017, 27(10), 1606129

[26] Tongay S, Sahin H, Ko C, et al. Monolayer behaviour in bulk ReS_2 due to electronic and vibrational decoupling. Nat Commun, 2014, 5, 3252

[27] Pradhan N R, McCreary A, Rhodes D, et al. Metal to insulator quantum-phase transition in few-layered ReS_2. Nano Lett, 2015, 15(12), 8377

[28] Lin Y C, Komsa H P, Yeh C H, et al. Single-layer ReS_2: two-dimensional semiconductor with tunable in-plane anisotropy. ACS Nano, 2015, 9(11), 11249

[29] Liu F, Zheng S, He X, et al. Highly sensitive detection of polarized light using anisotropic 2D ReS_2. Adv Funct Mater, 2016, 26(8), 1169

[30] Liu E, Long M, Zeng J, et al. High responsivity phototransistors based on few-layer ReS_2 for weak signal detection. Adv Funct Mater, 2016, 26(12), 1938

[31] Cao S, Xing Y, Han J, et al. Ultrahigh-photoresponsive UV photodetector based on a BP/ReS_2 heterostructure p–n diode. Nanoscale, 2018, 10(35), 16805

[32] Li X K, Gao X G, Su B W, et al. Polarization-dependent photocurrent of black phosphorus/rhenium disulfide heterojunctions. Adv Mater Interfaces, 2018, 5(22), 1800960

[33] Castellanos-Gomez A, Buscema M, Molenaar R, et al. Deterministic transfer of two-dimensional materials by all-dry viscoelastic stamping. 2D Mater, 2014, 1(1), 011002

[34] Perello D J, Chae S H, Song S, et al. High-performance n-type black phosphorus transistors with type control via thickness and contact-metal engineering. Nat Commun, 2015, 6, 7809

[35] Shim J, Oh S, Kang D H, et al. Phosphorene/rhenium disulfide heterojunction-based negative differential resistance device for multi-valued logic. Nat Commun, 2016, 7, 13413

[36] Jo S H, Lee H W, Shim J, et al. Highly efficient infrared photodetection in a gate-controllable Van der Waals heterojunction with staggered bandgap alignment. Adv Sci, 2018, 5(4), 1700423

[37] Massicotte M, Schmidt P, Vialla F, et al. Picosecond photoresponse in van der Waals heterostructures. Nat Nanotechnol, 2015, 11, 42

[38] Xue Y, Zhang Y, Liu Y, et al. Scalable production of a few-layer MoS_2/WS_2 vertical heterojunction array and its application for photodetectors. ACS Nano, 2016, 10(1), 573

[39] Lv Q, Yan F, Wei X, et al. High-performance, self-driven photodetector based on graphene sandwiched GaSe/WS_2 heterojunction. Adv Opt Mater, 2018, 6(2), 1700490

[40] Yan F, Zhao L, Patane A, et al. Fast, multicolor photodetection with graphene-contacted p-GaSe/n-InSe van der Waals heterostructures. Nanotechnology, 2017, 28(27), 27L

[41] Wei X, Yan F, Lv Q, et al. Fast gate-tunable photodetection in the graphene sandwiched WSe_2/GaSe heterojunctions. Nanoscale, 2017, 9(24), 8388

[42] Wei X, Yan F, Lv Q, et al. Enhanced photoresponse in $MoTe_2$ photodetectors with asymmetric graphene contacts. Adv Opt Mater, 2019, 0(0), 1900190

[43] Wu W, Zhang Q, Zhou X, et al. Self-powered photovoltaic photodetector established on lateral monolayer MoS_2-WS_2 heterostructures. Nano Energy, 2018, 51, 45

[44] Liu H, Xu B, Liu J M, et al. Highly efficient and ultrastable visible-light photocatalytic water splitting over ReS_2. Phys Chem Chem Phys, 2016, 18(21), 14222

[45] Huang S, Ling X. Black phosphorus: optical characterization, properties and applications. Small, 2017, 13(38), 1700823

[46] Ling X, Huang S, Hasdeo E H, et al. Anisotropic electron-photon and electron-phonon interactions in black phosphorus. Nano Lett, 2016, 16(4), 2260

[47] Wang X, Li Y, Huang L, et al. Short-wave near-infrared linear dichroism of two-dimensional germanium selenide. J Am Chem Soc, 2017, 139(42), 14976